Inelastic-neutron-scattering study of phonon eigenvectors and frequencies in Si

Jiří Kulda
Institut Laue-Langevin, 156X, 38042 Grenoble Cedex, France
and Nuclear Physics Institute, 25068 Řež near Prague, Czech Republic

Dieter Strauch and Pasquale Pavone
Institut fur Theoretische Physik, Universität Regensburg, Regensburg, Germany

Yoshinobu Ishii
Japan Atomic Energy Research Institute, Tokai-mura, Naka-gun, Ibaraki-ken 319-11, Japan
(Received 5 July 1994)

Longitudinal-acoustic and -optic phonons along the three main symmetry directions in Si were investigated by coherent neutron inelastic scattering. While the determination of phonon frequencies is a routine task, the complementary information on the phonon eigenvectors contained in the intensities of the observed phonon groups is exploited only rarely. The main reasons are problems with correct normalization and reliability of the data, caused by frequent occurrence of spurious peaks. In the present study we addressed this problem by restricting the experiment to scans fulfilling conditions for good resolution so that most of the observed phonon peaks could be resolved from the spurious ones. The inelastic structure factors were then extracted from several sets of integrated intensities, observed at different **Q** and ω values, and fitted by appropriate models with common scale factors in order to obtain detailed information on eigenvector phases and amplitudes in elliptically polarized modes. The observed eigenvectors and frequencies were found in good agreement with results of *ab initio* calculations.

I. INTRODUCTION

Usual measurements of dispersion relations of excitations in crystalline solids provide information on the eigenvalues of the corresponding dynamical matrix $D(\mathbf{q})$, whose eigenvectors then can be only inferred from symmetry conditions and from model calculations. As demonstrated by Leigh, Szigeti, and Tewary[1], to a given set of eigenvalues an infinite variety of eigenvectors can be attributed, resulting each time in a different set of force constants. A complete experimental study should thus comprise not only the determination of positions of observed inelastic peaks but also analysis of their integrated intensities in terms of inelastic structure factors containing information on the eigenvectors. This problem, although recognized since the early days of inelastic-neutron-scattering studies of lattice dynamics,[2,3] has proved rather difficult to solve in practice and as a result only few attempts to interpret the observed inelastic intensities quantitatively[4–7] have been reported.

Both Iizumi[5] working on CaF_2 and more recently Straugh, Mayer, and Dorner working[7] on silicon have found significant departures from sum rules quoting that the sum of intensities, scattered by the LA and LO modes at a given point in the Brillouin zone and belonging to the same irreducible representation, should be constant. These departures might have originated both from instrumental problems—observed profiles contaminated by spurious peaks and inadequacies in account of resolution effects—and from violations of the first Born approximation (kinematic approach) in description of the scattering process itself. Therefore in the initial stage of the present study we have verified the kinematic behavior of the observed inelastic intensities[8] for perfect silicon samples of thicknesses up to about 10 mm. Despite the extreme crystalline perfection of the employed crystals and a relatively large phonon lifetime in silicon, the observed intensities were found proportional to the irradiated crystal volume and insensitive to changes of the crystal quality (elastic deformation). In this paper we report the results obtained in further stages, when integrated intensities scattered by acoustic phonons along the three main symmetry directions in silicon have been measured.

Silicon has been chosen as the object of the present study for several reasons. On the one hand, samples of extremely high and well characterized crystalline quality can be prepared easily in virtually any shape, size, and orientation. On the other hand, silicon remains an interesting material from the point of view of lattice dynamics, a number of phenomenological models has been designed for its description, and in recent years quite extensive results of *ab initio* calculations have become available.[9] Moreover silicon has been subject to the abovementioned experimental study of the eigenvector phases of $[\xi\xi\xi]$ LA/LO phonons,[7] which despite problems with the sum rules, provided some reliable results that could serve as a reference point in the present work. Although our principal goal was the determination of inelastic structure factors, the observed frequencies of longitudinal acoustic and optic phonons form an important part of the results. Their most "recent" experimental values date back to the early 60's (Ref. 10) and exhibit excessive error bars so that the authors of a recent study of internal strain in semiconductors with the diamond structure[11]

preferred to replace the Si frequencies by rescaled Ge values.

II. INELASTIC STRUCTURE FACTORS

The lattice vibrations are described in terms of normal modes obtained by Fourier transformation of the real-space atomic displacements. In doing so certain ambiguity exists in the choice of the phase factors. If $\exp[i\mathbf{q}\cdot\mathbf{R}(l)]$, constant within a unit cell, is used, the displacement $\mathbf{u}(l,k)$ of the kth atom in the lth cell can be written in terms of a sum over all phonon wave vectors $\mathbf{q}$ and modes j as[13]

$$\mathbf{u}(l,k)=\sum_{\mathbf{q},j}\sqrt{\hbar/2\omega(\mathbf{q},j)NM_k}\,\mathbf{e}(k\,|\mathbf{q},j)\times\exp[i\mathbf{q}\cdot\mathbf{R}(l)](\hat{a}_{\mathbf{q},j}-\hat{a}^{\dagger}_{-\mathbf{q},j})\ . \quad (1)$$

Here N and M_k are the number of elementary cells per unit volume and the atomic mass, respectively, $\mathbf{e}(k\,|\mathbf{q},j)$ denotes the phonon polarization vector and $\hat{a}^{\dagger}_{\mathbf{q},j},\hat{a}_{\mathbf{q},j}$ are the creation/annihilation operators. For non-Bravais lattices the components of $\mathbf{e}(k\,|\mathbf{q},j)$ are generally complex, as they contain a geometrical phase $\exp[i\mathbf{q}\cdot\mathbf{d}(k)]$ for each atom. This can be avoided if the Fourier transform is performed with phase factors $\exp[i\mathbf{q}\cdot\mathbf{r}(l,k)]$, where $\mathbf{r}(l,k)=\mathbf{R}(l)+\mathbf{d}(k)$, and $\mathbf{d}(k)$ is the position vector of the kth atom with respect to the unit cell origin. In this case

$$\mathbf{u}(l,k)\approx\sum_{\mathbf{q},j}\boldsymbol{\sigma}(k\,|\mathbf{q},j)\exp[i\mathbf{q}\cdot\mathbf{r}(l,k)](\hat{a}_{\mathbf{q},j}-\hat{a}^{\dagger}_{-\mathbf{q},j}) \quad (2)$$

and the polarization vectors $\boldsymbol{\sigma}$ differ from $\mathbf{e}$ by the absence of the phase factor $\exp[i\mathbf{q}\cdot\mathbf{d}(k)]$.

In non-Bravais lattices the mutual positions of atoms in the unit cell are not fixed by point-group symmetry operations and hence may change whenever the unit cell gets deformed. These shifts of atomic positions result in additional variations of the eigenvector phases. In what follows we shall denote the phases corresponding to the $\mathbf{e}$ and $\boldsymbol{\sigma}$ conventions by ϕ and Φ, respectively, with

$$\phi(\mathbf{q})=\Phi(\mathbf{q})+\mathbf{q}\cdot\mathbf{d}(k)\ . \quad (3)$$

The use of the $\mathbf{e}$ convention is convenient in the context of lattice dynamics as all the information on the phases of motion of the individual atoms within the unit cell is kept in the polarization vectors. On the other hand in the context of the present work, which we understand as an extension of the conventional methods of structure analysis into the time-dependent domain, the use of the $\boldsymbol{\sigma}$ convention is logical as it permits us to write the inelastic structure factor as

$$f(\boldsymbol{\tau}+\mathbf{q})=\sum_k\frac{\mathbf{Q}\cdot\boldsymbol{\sigma}_k}{Q}\frac{b_k}{\sqrt{m_k}}\exp[i(\boldsymbol{\tau}\cdot\mathbf{d}(k)+\Phi_k(\mathbf{q}))]\ , \quad (4)$$

where $\boldsymbol{\tau}$ is a reciprocal-lattice vector and the phase Φ_k for each atom represents just the departure from the crystallographic phase relevant to the Bragg point at the origin of the Brillouin zone (BZ). Whatever convention adopted, it is important to note that the phase term in Eq. (4) represents the interference between the geometrical phase $\boldsymbol{\tau}\cdot\mathbf{d}_k$ and the phonon phase Φ_k. Hence *for a known crystal structure the phonon phases can always be determined by measuring intensities in appropriately chosen Brillouin zones.*

The inelastic structure factors enter the experimentally observed integrated intensities of coherent inelastic scattering. In the case of a three-axis spectrometer, equipped with a monitor whose efficiency is proportionate to k_0^{-1}, and for measurements carried out with a fixed final neutron wave vector,[12] the observed intensity of neutron energy loss scattering is given by

$$I_{\rm obs}=I_0\frac{V\langle n+1\rangle\hbar}{V_0^2 2\omega(\mathbf{q})}\exp[-2W(Q)]\frac{Q^2}{J(\mathbf{Q})}|f(\mathbf{Q})|^2\ , \quad (5)$$

where all the symbols have their usual meaning.[13,14] In particular, $J(Q)$ is the Waller-Froman Jacobian

$$J=\left|1+\frac{1}{2\omega}\mathbf{k}\cdot\nabla_q\omega(\mathbf{q})\right| \quad (6)$$

being equal to $v_g\cos\chi$ for the $E=$const. scans with v_g and χ representing the phonon group velocity and the angle between scan direction and $\nabla_q\omega$; in our case always $\chi=0$. For the $Q=$const. scans this Jacobian is equal to unity.

III. EXPERIMENTS

The silicon samples were prepared from zone-melted, low-doped, dislocation-free single-crystal ingots grown in the [100] and [111] directions by Wacker Chemitronic (FRG). An approximate cylinder of 10 mm diameter with axis along ⟨110⟩ and several plane-parallel plates of different thicknesses (1 to 15 mm) and surface orientations were cut with a diamond saw and the damaged surface layer ($\approx 10\mu$m) was etched down. In the final stage of the integrated intensity measurements platelike samples of about 5 mm thickness and the cylinder were used.

The inelastic-neutron-scattering experiments were performed at the JRR-3M reactor (20 MW, 3×10^{14} n cm^{-2} s^{-1}) at the Japan Atomic Energy Research Institute (JAERI, Tokai, Japan) on the TAS-1 three-axis spectrometer. A vertically focusing pyrolithic graphite (PG) (002) monochromator and a flat PG(004) analyzer were used together with beam collimations 40′-20′-40′-40′. The final neutron momentum was fixed throughout most of the experiments at $k_f=4.482$ Å^{-1} ($E_f\cong 10$ THz). Only part of the optic-phonon measurements has been performed with the PG(002) analyzer and different smaller k_f values, fixed through individual scans. All the experiments were carried out at room temperature (297 K) in the neutron energy-loss regime.

IV. EXPERIMENTAL RESULTS

A. Phonon frequencies

The [00ξ], [$\xi\xi$0], and [$\xi\xi\xi$] phonons were measured in order to determine both their frequencies and polarization vectors. The data were collected in the course of

TABLE I. Phonon frequencies in Si observed in the present work.

[ξ00] ξ	ν(LA) [THz]
0.180	3.00±0.04
0.250	4.00±0.03
0.319	5.00±0.03
0.393	6.00±0.01
0.475	7.00±0.03
0.559	8.00±0.02
0.647	9.00±0.02
0.739	10.00±0.02

[ξξ0] ξ	ν(Σ1) [THz]	ξ	ν(Σ3) [THz]
0.079	2.00±0.05	0.207	3.00±0.02
0.121	3.00±0.01	0.408	5.20±0.02
0.170	4.00±0.01	0.499	6.00±0.02
0.225	5.00±0.01	0.599	6.73±0.02
0.238	5.20±0.01	0.699	6.99±0.02
0.287	6.00±0.01	0.817	6.00±0.02
0.358	7.00±0.02	0.894	5.20±0.01
0.400	7.50±0.01		
0.445	8.00±0.01		
0.539	9.00±0.01		
0.640	10.00±0.01		
0.691	10.50±0.02		
0.798	11.43±0.01		
0.899	12.08±0.02		

[ξξξ] ξ	ν(LA) [THz]
0.095	3.00±0.01
0.132	4.00±0.01
0.171	5.00±0.01
0.211	6.00±0.01
0.253	7.00±0.01
0.297	8.00±0.02

[ξ00] ξ	ν(LA) [THz]
0.345	9.00±0.02
0.396	10.00±0.02
0.425	10.50±0.02
0.480	11.33±0.01
0.500	11.42±0.08

[ξ00] ξ	ν(LO) [THz]	ν(TO) [THz]
0.00		15.69±0.07
0.20	15.55±0.04	15.39±0.05
0.40	15.22±0.02	24.58±0.04
0.60	14.61±0.04	14.34±0.02
0.80	13.77±0.06	13.59±0.04
1.00	12.45±0.02	13.69±0.13

[ξξ0] ξ	ν(Σ1) [THz]	ν(Σ3) [THz]
0.20	14.96±0.04	15.05±0.02
0.40	14.82±0.08	13.63±0.01
0.60	14.36±0.11	11.84±0.02
0.80	14.44±0.05	11.39±0.02
1.00	13.89±0.06	12.33±0.01

[ξξξ] ξ	ν(LO) [THz]	ν(TO) [THz]
0.10	15.26±0.06	15.58±0.05
0.20	14.89±0.01	15.53±0.08
0.30	14.32±0.02	14.98±0.04
0.40	13.41±0.02	14.91±0.02
0.45	12.78±0.01	
0.48	12.50±0.01	
0.50	12.33±0.01	14.62±0.28

three independent experiments using the same spectrometer setup but different Si samples. In all cases the incident wavelength was calibrated using an ASTM silicon powder standard, and the samples were carefully aligned so that the observed positions of the various 440 and 004 Bragg peaks did not differ by more than 2×10^{-3} r.l.u. from the calculated ones in any direction. As a result the frequencies measured for the same phonon in different experiments in most cases coincided within the error bars of the order of 0.01 THz. The final results are given in Table I and in Fig. 1, for acoustic phonons each frequency represents a mean of several values, observed in different BZ's and/or on different samples, so that the errors are estimated from the variances of these miniensembles.

In addition to the acoustic phonons we have also remeasured the frequencies of the optic phonons with polarization vectors lying in the $(1\bar{1}0)$ plane. Up to a few exceptions the new frequencies lie within the error bar band of the previously reported ones.[7,10,15] The only significant deviation was found for the [ξξξ] TO phonons near to the zone boundary, where the actual results did not confirm the dip observed by Dolling at $\xi\approx0.4$.

B. Inelastic-scattering intensities

For methodical reasons two different procedures for the measurement of integrated intensities were tested. Initially, we have used $E=$const scans which permitted to keep the resolution volume of the spectrometer constant and thus to facilitate the normalization of the observed intensities, which were only compared within data sets collected at a given energy transfer. In these runs samples in the form of plane-parallel plates 5 mm thick, covering the whole incident-beam cross section, were used. In such a way the data for the LA phonons along [00ξ] and [ξξξ] were collected. The integrated intensities were determined by fitting a (multi-)Gaussian profile

to the observed peaks, in most cases they corresponded to 500–1000 counts. Next the structure factors were extracted from the integrated intensities with the help of Eq. (5). Absorption correction based on the energy-dependent total cross section reported by Freund[16] has been tested, but its effect (1–2%) remained within the data error bars.

Figure 2 displays the inelastic structure factors as refined from sets of intensity data collected at the given energy transfers in four different BZ's: 224, 115, 333, and 335. Each set of eight structure factors observed at a given energy transfer between 3 and 10 THz was then fitted by a model corresponding to Eq. (4) with the phase $\Phi(\xi)$ as a free parameter. At energy transfers below 6 THz it proved necessary to include a separate scale factor for the $[\xi\xi\xi]$ phonons being up to 13% higher than that for the $[00\xi]$ branch. Taking into account this increase in intensity (most probably due to differences in scattering surface curvature) had, anyway, only negligible influence on the refined phase values $\Phi(\xi)$ given in Fig. 3(b) in the form of $\phi(\xi)=\Phi(\xi)+\frac{3}{2}\pi\xi$ [cf. also Eq. (3)].

Encouraged by these results, in a subsequent stage we turned towards a more straightforward procedure: for the $[\xi\xi 0]$ Σ_1 and Σ_3 acoustic branches we employed a cylindrical sample having its vertical axis along [110] and a diameter of about 10 mm, so that it was completely and uniformly bathed in the incident beam throughout all of the scans. The incident (monochromatic) beam monitor was calibrated to give proper measure of the flux incident on the sample. Under these conditions both $E=$const and $\mathbf{Q}=$const scans were used in dependence on the slope of the phonon-dispersion curve. Data for a total of 63 points in six different BZ's have been collected. As in the preceding case, integrated intensities of the observed phonon peaks were determined by fitting (multi-)Gaussian profiles and contributions from spurious peaks were discarded. In three cases it proved impossible to resolve the observed phonon peak from a spurious one, these points were discarded from further treatment. In a subsequent step all the experimental intensities belonging to the $[\xi\xi 0]$ Σ_1 and Σ_3 branches were fitted by a model based on the theoretical *(ab initio)* eigenvectors and containing a single, common scale factor. As this procedure is in direct analogy to the structure refinement procedures used in crystallography, we used the agreement factor, defined as

$$R_1=\frac{1}{N}\sum\frac{f_{\rm obs}-f_{\rm calc}}{f_{\rm calc}}$$

to measure the quality of the fit. The resulting value was $R_1=4.8\%$, comparable to the accuracy obtained with Bragg scattering. Several examples of the inelastic structure factors observed in different BZ's are given in Figs. 4, 5(a), and 6(a).

V. OBSERVED PHONON EIGENVECTORS ALONG [100] AND [111]

The diamond lattice consists of two fcc sublattices mutually shifted by $\frac{1}{4}$ of the space diagonal of the cubic unit cell. As a result all of the atoms of one sublattice can be considered as sitting in the centers of regular tetrahedra having in vertices the atoms of the second sublattice. This position, although apparently symmetric, does not contain all the point-group symmetry of the fcc lattice—namely the center of symmetry is absent. As a result, under stress applied to the unit cell, the atoms may get displaced from the center of the tetrahedron depending on the modified equilibrium of the bonding forces. This effect—the internal strain—appears already under static applied stress and has been studied by x-ray diffraction.[17] In the case of the LA phonons the deformation of the unit cell is much stronger and the displacements $\Delta\mathbf{u}$ of the central atom become translated into an additional phase shift $\Phi=\mathbf{q}\cdot\Delta\mathbf{u}$ entering the structure factors in different zones as

$$f(\mathbf{Q})=f_0\{1+\exp[-i((h+k+l)\pi/2+\Phi)]\}\ . \qquad (7)$$

Obviously, a given $\Phi(\xi)$ dependence produces different variations of the structure factor magnitudes in Brillouin zones having different sums of the Miller indices.

In the [100] (Δ) direction the stress due the longitudinal phonons is symmetric, as on each side of any (100) plane there remain two bonds at the same angles (twisted around [100] by 90° with respect to the other pair). As a

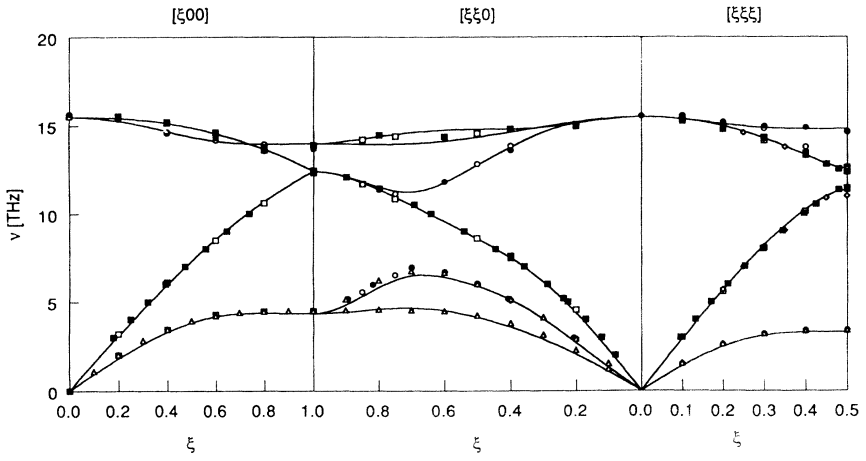

FIG. 1. The phonon frequencies in silicon: the full symbols (■,●) represent the results of the present work, while the open ones correspond to the previous results of Dolling (Ref. 10) (□,○), Nilsson and Nelin (Ref. 15) (△) and Strauch, Mayer, and Dorner (Ref. 7) (◇) (error bars —unless plotted— are smaller than symbol size).

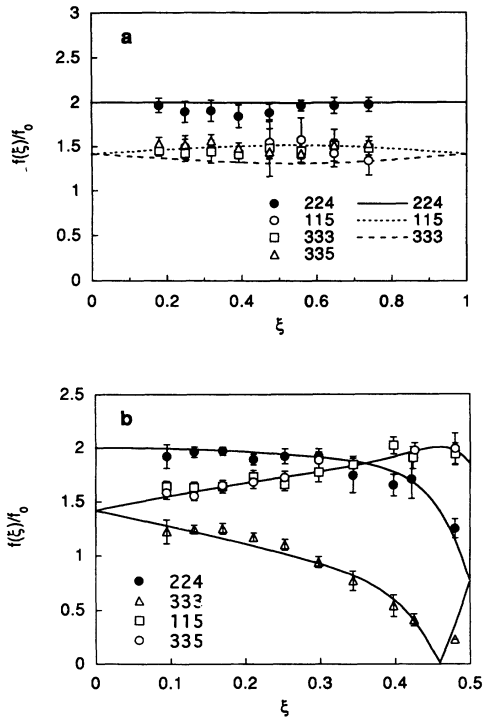

FIG. 2. The normalized inelastic structure factors $f(\mathbf{Q})/f_0$ for the LA phonons along $[\xi 00]$ (a) and $[\xi\xi\xi]$ (b) observed in four different Brillouin zones. The solid lines connect values corresponding to the refined phases (cf. Fig. 3).

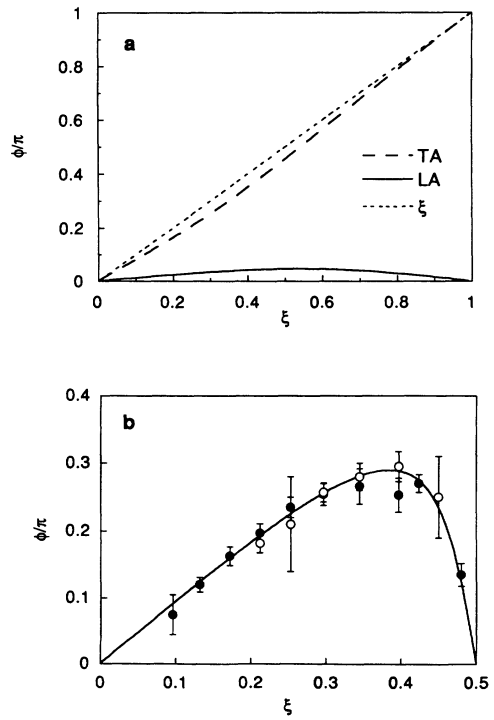

FIG. 3. The phase ϕ of the polarization vectors of $[\xi 00]$ LA (a) and $[\xi\xi\xi]$ LA (b) phonons: present results (●) in comparison with those of Strauch, Mayer, and Dorner (○) and the prediction of the *ab initio* calculations (solid line).

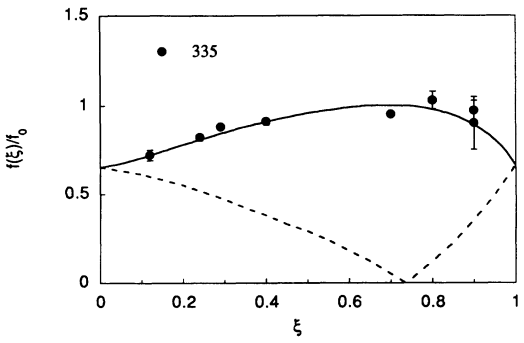

FIG. 4. The normalized inelastic structure factors $f(\mathbf{Q})/f_0$ for the $[\xi\xi 0]$ Σ_1 elliptically polarized phones (●) as observed in the 335 Brillouin zone. The solid curve corresponds to polarization vectors from *ab initio* calculations; the dashed curve corresponds to the inverted sense of rotation.

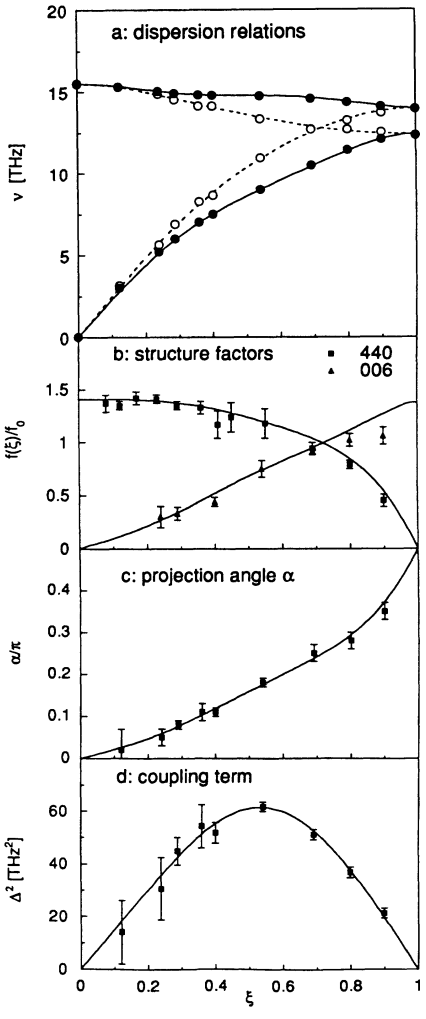

FIG. 5. Coupling of the Σ_1 phonon branches in silicon: frequencies (a) (error bars are smaller than symbol size), structure factors in selected BZ's (b), projection angle α of the polarization vector on the [110] direction (c) and the coupling term Δ^2 (d); the smooth curves represent the results of *ab initio* calculations.

result, the mutual position of the two atoms of the basis remains preserved in the distorted unit cell and no appreciable eigenvector phase Φ should be observed. This is in accord with the measured inelastic structure factors for the [100] LA phonons displayed in Fig. 2(a), whose values remain approximately constant throughout the Brillouin zone. The small nonzero phase displayed in Fig. 3(a), resulting in the *ab initio* calculations, lies below the detection limit in the present experiments.

Unlike the [100] (Δ) direction, for LA phonons along [111] the asymmetry of the tetrahedral bonding is fully manifested: on one side of each (111) plane there remains a single bond parallel to [111] and strained purely radially, while on the opposite side of the plane there are three bonds (along $[1\bar{1}\bar{1}]$, etc.) inclined at an angle of 70.5° and hence strained predominantly in tangential direction. The displacement of atoms from the central position in the tetrahedron, observable via the eigenvector phase $\Phi(\xi)$ in Eq. (7), becomes a direct measure of the balance between the radial and tangential bond strengths. In Fig. 2(b) we present the data observed in the four BZ's, 224, 333, 115, and 335, used to determine the phase function $\Phi(\xi)$. In particular, from the general trends of the data observed in BZ's with odd indices, $h+k+l=4n\pm1$, a negative sign of $\Phi(\xi)$ can be concluded. In order to facilitate comparison with the previously published result, we give in Fig. 3(b) the function $\phi(\xi)=\Phi(\xi)+\frac{3}{2}\pi\xi$ (cf. also Eq. 3). Both the absolute values and the sign agree with the previous results obtained on silicon[7] as well as with the results of our *ab initio* calculations. In more qualitative terms, the observed $\Phi(\xi)<0$ implies that the radial strength of the covalent bond in Si (similarly to Ge) is larger than the tangential one as opposed to the case of diamond, where the *ab initio* calculations[9] predict $\phi(\xi)>3\pi/2$ equivalent to $\Phi(\xi)>0$.

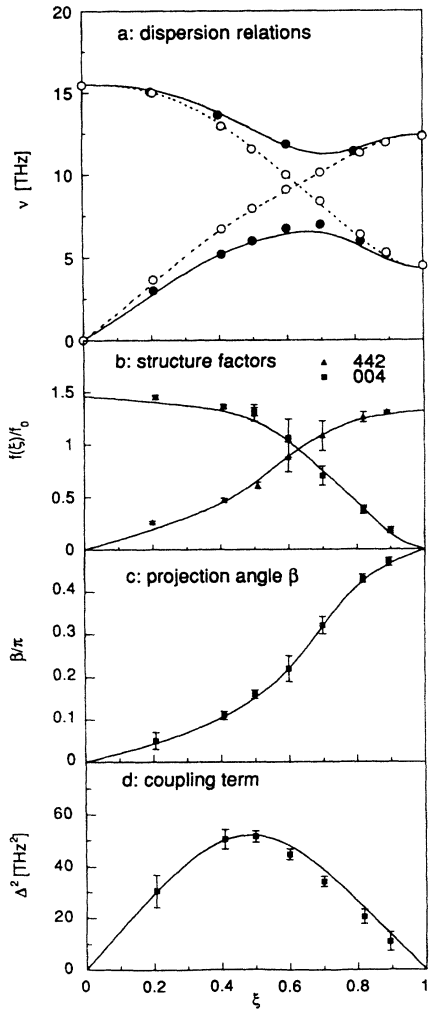

FIG. 6. Coupling of the Σ_3 phonon branches in silicon: frequencies (a) (error bars are smaller than symbol size), structure factors in selected BZ's (b), projection angle β of the polarization vector on the [110] direction (c) and the coupling term Δ^2 (d); the smooth curves represent the results of *ab initio* calculations.

VI. COUPLED BRANCHES ALONG [110]

Similarly to the Δ direction, in the [110] (Σ) direction the phase of the displacement of each atom is given by just $\exp[-i\mathbf{q}\cdot\mathbf{d}(k)]$ so that the phase Φ of Eq. (7) is zero throughout the BZ. On the other hand, the polarization of the Σ_1 and Σ_3 modes is elliptic, varying from longitudinal at zone origin to transverse at zone boundary and vice versa. At the same time also the character of these branches changes, e.g., the low-energy branches are acoustic at zone origin and optic at zone boundary. Their eigenvectors can be written as

$$\sigma_1=\sigma_{011}\sin(\alpha)+i\sigma_{100}\cos(\alpha) -[\sigma_{011}\sin(\alpha)-i\sigma_{100}\cos(\alpha)]\exp(-i\pi\xi) \quad (8)$$

in the case of Σ_1 and as

$$\sigma_3=\sigma_{011}\cos(\beta)-i\sigma_{100}\sin(\beta) +[\sigma_{011}\cos(\beta)+i\sigma_{100}\sin(\beta)]\exp(-i\pi\xi) \quad (9)$$

in the case of Σ_3. Obviously, the eigenvectors of the corresponding high-energy branches (optic at zone origin) can be obtained by replacing $\cos\rightarrow-\sin$ and $\sin\rightarrow\cos$ in Eqs. (8) and (9). All these features are reflected in the inelastic structure factors. Inserting these polarization vectors into Eq. (4), we see that in Brillouin zones with even indices we have

$$f(\mathbf{Q})\approx 2\mathbf{Q}\cdot\sigma_{011}\sin(\alpha) \quad (10)$$

in the case of $h+k+l=4n$ and

$$f(\mathbf{Q})\approx 2\mathbf{Q}\cdot\sigma_{100}\cos(\alpha) \quad (11)$$

in the case of $h+k+l=4n+2$ permitting to determine directly the polarization vector projections on the two symmetry directions.

The same operation in zones with odd Miller indices yields

$$f(\mathbf{Q})\approx(1\pm i)[\mathbf{Q}\cdot\sigma_{011}\sin(\alpha)\mp\mathbf{Q}\cdot\sigma_{100}\cos(\alpha)] \quad (12)$$

for $h+k+l=4n\pm1$. As a result the absolute value of the structure factor in BZ's with odd indices is sensitive to the mutual sign of the [110] and [001] components of the polarization vectors in Eqs. (8) and (9), which means that we are able to detect the sense of rotation in the case of elliptical polarization. This is demonstrated in Fig. 4 displaying the structure factors observed in the 335 zone and corresponding to the Σ_1 acoustic branch; a dotted line represents $f(\xi)/f_0$ calculated with the *ab initio* eigenvectors, but having the reversed sense of rotation.

Figures 5(a), 5(b), 6(a), and 6(b) display the observed frequencies and structure factors for the pairs of the Σ_1 (LA/TO1) and Σ_3 (LO/TA1) branches, respectively. In analogy to the conventional quantum-mechanical treatment of band crossings,[18] we may describe the coupling of each pair by an eigenvalue equation with a reduced, 2×2 dynamical matrix

$$\begin{bmatrix} \varepsilon_1^2 & \Delta^2 \\ \Delta^2 & \varepsilon_2^2 \end{bmatrix} \begin{bmatrix} w_1 \\ w_2 \end{bmatrix} = \nu^2 \begin{bmatrix} w_1 \\ w_2 \end{bmatrix} , \tag{13}$$

where $\varepsilon_{1,2}$ are the original unperturbed frequencies, Δ is the coupling constant, and $w_{1,2}$ are the coefficients of the two polarization components. The modified eigenfrequencies, observed in the experiment, are then given by

$$\nu_{1,2}^2=[\varepsilon_1^2+\varepsilon_2^2\pm\sqrt{(\varepsilon_1^2-\varepsilon_2^2)^2+4\Delta^4}]/2 . \tag{14}$$

The corresponding pair of hybridized eigenfunctions can be written as

$$\psi_1=\varphi_1\cos\chi+\varphi_2\sin\chi ,$$

$$\psi_2=-\varphi_1\sin\chi+\varphi_2\cos\chi , \tag{15}$$

where the projection angle χ is defined through

$$\tan2\chi=2\Delta^2/(\varepsilon_1^2-\varepsilon_2^2) \tag{16}$$

and φ_1,φ_2 are the wave functions of the unperturbed states. In our case they correspond to the acoustic- and optic-phonon modes with pure longitudinal or transverse polarizations entering the right-hand sides of Eqs. (8) and (9). The projection angle χ equal to one of the angles α, β whose experimental values are displayed in Figs. 5(c) and 6(c).

The fact that we have experimentally determined not only the frequencies of the $[\xi\xi0]$ Σ_1 and Σ_3 branches but also the projection angles α, β of the polarization components permits us now to reconstruct the complete dynamical matrix in the left-hand side of Eq. (13). We only need to establish the relation between the observed quantities and the coupling term Δ^2. Combining Eqs. (14) and (16) we find after some algebraic manipulations of the sum and of the difference of Eq. (14) that

$$\Delta^2=\frac{\nu_1^2-\nu_2^2}{2}\sin2\chi \tag{17}$$

and

$$\varepsilon_{1,2}^2=\frac{\nu_1^2+\nu_2^2}{2}\pm\Delta^2\cot2\chi . \tag{18}$$

The unperturbed frequencies $\varepsilon_{1,2}$ are plotted in Figs. 5(a) and 6(a) together with the observed frequencies $\nu_{1,2}$, while Figs. 5(d) and 6(d) display the resulting values of the coupling parameter Δ^2 for the Σ_1 and Σ_3 branches. The fact that the coupling between, e.g., the Σ_1 (LA/TO1) modes extends over the whole BZ is consistent with the previous conclusion about the dominant role of the bond bending in deformation of the tetrahedral cell of silicon. In such a case the longitudinal deformation along [110] implies a transversal movement of the central atom along [001] which in turn provokes bending of its bonds in the $(11\bar{1})$ plane. In this way the longitudinal-acoustic mode is always accompanied by a movement corresponding to a transverse-optic mode.

VII. CONCLUDING REMARKS

The present results demonstrate the feasibility of exploitation of the information contained in intensities of coherent inelastic scattering. Unlike analogous preceding experiments we were able to utilize practically all of the experimental intensity data, as from the complete set of the 117 observed structure factors only a few (5) values had to be discarded because of large departures from those predicted by the ensemble average. The overall agreement factor between calculated and observed structure factors stayed well around 5%—a situation which is not very different from that met in crystallography. Within this accuracy and for the chosen phonon branches the present experimental results provide exhaustive information on the lattice dynamics of silicon, equivalent to a reconstruction of the dynamical matrix.

Comparing the obtained experimental results with predictions from the *ab initio* calculations we find that the phonon eigenvectors agree within error bars with the computed ones, while there are observed some significant departures for the frequencies. It should, however, be noted that the calculations are performed in fact for a purely harmonic crystal at 0 K, while the experiment has been performed at room temperature and, of course, the error bar margins for the frequencies are much narrower.

ACKNOWLEDGMENTS

The experimental part of this work was enabled by JAERI's Foreign Researcher Inviting Programme which provided travel funds for one of the authors (J.K.). It is a pleasure to acknowledge the kind support of S. Funahashi (JAERI) and B. Dorner (ILL) through all stages of this project, fruitful discussions with M. Iizumi (JAERI), help of S. Katano (JAERI) as well as the expert technical assistance of N. Minakawa and Y. Shimojio during the experiments. The silicon samples were kindly donated by Dr. W. Zulehner from Wacker Chemitronic (FRG).

[1]R. S. Leigh, B. Szigeti, and V. K. Tewary, Proc. R. Soc. London, Ser. A **320**, 505 (1971).
[2]A. J. E. Foreman and W. M. Lomer, Proc. Phys. Soc. London **70**, 1143 (1957).
[3]B. N. Brockhouse, L. N. Becka, K. R. Rao, and A. D. B. Woods, in *Inelastic Scattering of Neutrons in Solids and Liquids* (IAEA, Vienna, 1963), Vol. 1, p. 23.
[4]J. D. Axe and G. Shirane, Phys. Rev. B **1**, 342 (1970).
[5]M. Iizumi, J. Phys. Soc. Jpn. **33**, 647 (1972).
[6]H. Boysen, B. Dorner, F. Frey, and H. Grimm, J. Phys. C **13**, 6127 (1980).
[7]D. Strauch, A. P. Mayer, and B. Dorner, Z. Phys. B **78**, 405 (1990).
[8]J. Kulda, D. Strauch, and Y. Ishii (unpublished).
[9]P. Giannozi, S. Gironcoli, P. Pavone, and S. Baroni, Phys. Rev. B **43**, 7231 (1991).
[10]G. Dolling, in *Inelastic Scattering of Neutrons in Solids and Liquids* (Ref. 3), p. 37.
[11]P. Molinas-Matta and M. Cardona, Phys. Rev. B **43**, 9799 (1991).
[12]B. Dorner, Acta Crystallogr. A **28**, 319 (1972).
[13]G. Dolling and V. F. Sears, Nucl. Instrum. Methods **106**, 419 (1973).
[14]S. W. Lovesey, *Theory of Neutron Scattering from Condensed Matter* (Clarendon, Oxford, 1984), Vol. 1.
[15]G. Nilsson and G. Nelin, Phys. Rev. B **6**, 3777 (1972).
[16]A. K. Freund, Nucl. Instrum. Methods **213**, 495 (1983).
[17]C. S. G. Cousins, L. Gerward, J. Staun Olsen, B. Selsmark, and B. J. Sheldon, J. Appl. Crystallogr. **15**, 154-9 (1982); C. S. G. Cousins, L. Gerward, J. Staun Olsen, B. Selsmark, and B. J. Sheldon, J. Phys. C **20**, 29 (1987).
[18]A. S. Davydov, *Quantum Mechanics* (Pergamon, Oxford, 1965).